JMEPEG (2011) 20:1304–1309
DOI: 10.1007/s11665-010-9752-8

1059-9495/$19.00

Magnetic Properties and Nanocrystalline Phases in Sn Containing $SmCo_5$ Alloys

Hamid Zaigham and F. Ahmad Khalid

(Submitted February 12, 2010; in revised form July 19, 2010)

$SmCo_5$ alloys with Sn additions (0.2-2.0 at.%) were prepared by mechanical milling of arc-melted samples. The nano-phase structures and magnetic properties of as-milled powders were investigated. The Sn additions resulted in development of nanocrystalline structures producing exchange-coupled magnets with better remanence magnetization to maximum magnetization ratios (M_r/M_{max}), typically 0.92 at 9.9 kOe coercivity. In addition, it was observed that the Sn concentrations lead to higher M_r/M_{max} ratios and maximum magnetization accompanying lower coercivity. X-ray diffraction revealed formation of 2:17 and 2:7 phases in 1:5 matrix, which were found to be dependent on Sn percentage. It appeared that higher Sn concentrations promoted 2:17 phase and helped in the formation of nano-sized phases.

Keywords coercivity, exchange interactions, mechanical milling, nanocrystalline phases, permanent magnet

1. Introduction

Rare earth magnets based on NdFeB when developed in 1980s, having augmented coercivity, higher energy product (BH_{max}), and lower cost drew the attention of the researchers from all over the world. However, the associated low Curie temperature limited their use in high temperature applications. Research efforts of last two decades could not result in any significant improvement in their Curie temperature, which resulted in refocusing research on magnets based on Sm-Co to increase their saturation magnetization without compromising coercivity. Hence, the Sm-Co magnets, especially based on 1:5 phase with $CaCu_5$-crystal structure, showing excellent bulk coercivity, high Curie temperature, lower temperature coefficient of coercivity and magnetization remain the main working horse for the high temperature applications. Coercivity mechanism in $SmCo_5$ system depends on control over nucleation of reverse domains and their subsequent growth at second phase and defects densities (Ref 1-4). The coercivity enhancement in $SmCo_5$ system is usually achieved by microstructural modification (Ref 5) and by reduction in the defect density in the lattice of $SmCo_5$ phase as a result of post-sintering heat treatments (Ref 6).

Previously, some researchers reported better coercivity values (2.4 MA/m or 30 kO_e) by the addition of Cu in $SmCo_5$ alloys treated at low post-sintering temperatures. Cu addition caused domain pinning at the grain boundaries by forming inter-metallic compounds. The Cu substitution in $SmCo_5$ alloys resulted in low saturation magnetization owing to the reduction in magneto-crystalline anisotropy (Ref 7-9).

Hamid Zaigham and **F. Ahmad Khalid**, Faculty of Materials Science and Engineering, GIK Institute of Engineering Sciences and Technology, Topi, KP, Pakistan. Contact e-mail: khalid@giki.edu.pk

Sn addition in $SmCo_5$ compound was first exploited in as cast alloy by Washko et al. (Ref 10). It resulted in shifting of crystallization structure from 1:5 to 2:17 and the resulting magnetic properties were found inferior to that of binary $SmCo_5$ alloys. Recently, Sn addition in melt spun samarium rich stoichiometric composition of $SmCo_5$ alloy has shown promising magnetic properties, in melt spun ribbons, having coercivity of 2.54 MA/m (32kOe) with a maximum energy product (BH)max of 65.6 kJ/m^3 (8.2 MGO_e). The phase 1:7 with Sn addition has shown increased saturation magnetization of 0.83 T (664 kA/m) and low coercivity of 1.38 kO_e (110 kA/m). The reason for high coercivity, in the hyper stoichiometric composition with lower Sn concentration, is the formation of non-magnetic grain boundary phase and separated particles acting as pinning sites (Ref 11).

It is pertinent to report that mechanical milling was effectively used to produce nanostructures in magnetic materials (Ref 12). Furthermore presence of nanocrystalline phases in magnetic materials can bring improvement in properties such as M_r/M_s ratio and domain interactions as compared to the conventional alloys (Ref 13, 14).

In the present work, role of Sn additions on the mechanically milled $SmCo_5$ powders are studied which is not reported previously. Attempt is made to explain the beneficial effects of the Sn addition which has also promoted nucleation of nano-sized 2:17 phase in 1:5 matrix thus producing superior magnetic properties.

2. Experimental

The hyper stoichiometric compositions containing Sn were selected for preparation of $SmCo_{5-x}Sn_x$ (x = 0.01, 0.06, and 0.12) ternary alloys. The alloys were prepared in a DC arc button furnace under flowing argon along with activated calcium placed in the closed vicinity of the melt cavity as gettering element to minimize the losses of Sm. The composition of alloys was determined by energy dispersion spectrum (EDS) measurements in scanning electron microscope and

Table 1 EDS composition analyses of as cast alloys

Sample	x	Bulk composition, at.%		
		Sm	Co	Sn
Alloy 1	0.01	17.73	82.04	0.23
Alloy 2	0.06	17.46	81.42	1.13
Alloy 3	0.12	16.86	80.95	2.17

shown in Table 1. The alloys were ground to pass through 500 μm sieve under flowing argon in a gloves box. The crushed material was then milled in planetary ball mill in argon environment with ball to charge ratio of 10:1 at 130 rpm for 240 min. The tungsten carbide balls of 10 mm diameter were used. The milling was interrupted for 10 min after each milling time of 10 min to avoid alloy decomposition due to milling generated heat. Finally, the material was milled in ethanol for 10 min to release material smeared onto the jar and balls. The handling of milled powder was carried out in the gloves box in an argon atmosphere.

The powder, sealed in the latex tube of 10 mm diameter and 150 mm length, was subjected to magnetic alignment by giving several pulses in a pulsed field coil of energy capacity of 1800 kJ. Then aligned powder samples were compressed at an isostatic pressure of 300 MPa. The samples were cut and impregnated with epoxy to consolidate the green compacts. The magnetic properties were measured using a pulsed field magnetometer of 10 T field. For x-ray diffraction analysis (XRD), transverse specimens were prepared have same experimental conditions (i.e., milling time and compaction load) from magnetically aligned green compacted rods. The samples were analyzed using x-ray diffractometer with Co source and crystallite size was investigated by x-ray integral breadth method (Ref 15, 16). To prepare samples for transmission electron microscope (TEM) studies, the milled powder was ultrasonically suspended in analytical grade ethanol. The suspended powder was coated on carbon-coated copper grid by droplet method, which was subsequently evaporated and dried. A 200 kV TEM was used for microstructural investigations.

3. Results and Discussion

Figure 1(a, b) illustrates the XRD patterns of samples tested in both random and aligned magnetic field conditions. The patterns indicate phases such as 1:5, 2:17, and 2:7 (JCPDS-ICDD card No: 35-1400, 35-1368 and 71-0387, respectively). Figure 1(b) shows the XRD patterns of the aligned green compact samples having a preferred orientation (002) along [001], which is considered as an easy magnetization direction. The patterns reveal presence of 1:5 phase with $CaCu_5$ structure type (ST). The alloys 1 and 2 reveal the nucleation of 2:7 phase (Ce_2Ni_7 ST) in the 1:5 matrix along with reduced intensities of 2:17 (Th_2Ni_{17} ST) reflections. Alloy 3 reveals pronounced formation of 2:17 phase in 1:5 matrix following a common c-axis along (002) plane. The result is in consistent with previously reported observation that Sn has a tendency to promote formation of 2:17 phase (Ref 10). However, the presence of 1:7 phase of $TbCu_7$ type crystal structure in melt spun ribbons can be attributed to distorted structure as reported

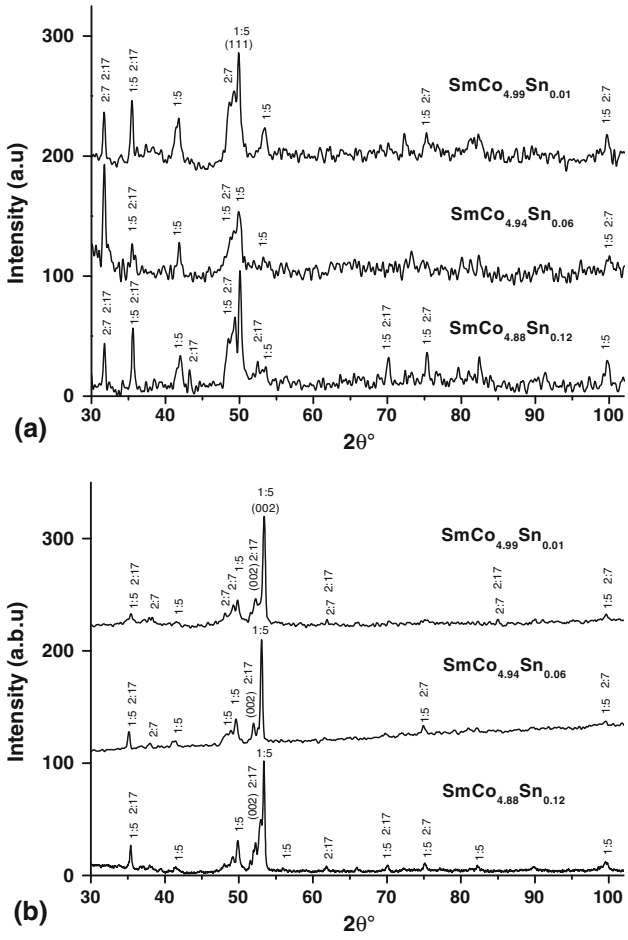

Fig. 1 XRD patterns of green compacted samples of alloys 1-3 (a) random and (b) magnetically aligned

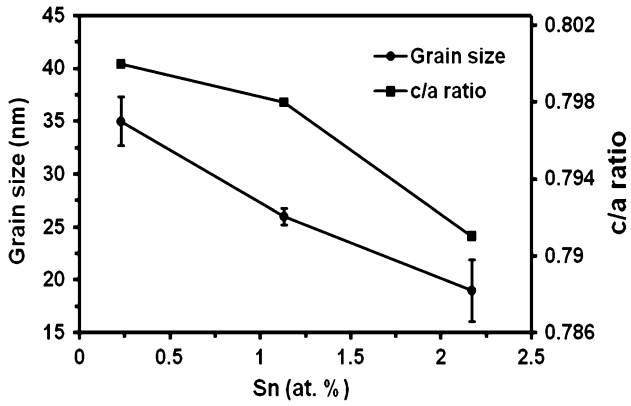

Fig. 2 Dependence of both the grain size and c/a ratio on Sn contents for $SmCo_{5-x}Sn_x$ alloy system

by Kundig et al. (Ref 11). The absence of reflections (006) and (204) for 2:17, may indicate the presence of 1:7 phase. However, due to low intensities and small fraction of 2:17; the absence of these peaks may not be the confirmation of 1:7 (Ref 17). The lattice parameters were determined from XRD. The c/a ratio decreased from 0.800 to 0.791 with increasing Sn concentration as shown in Fig. 2.

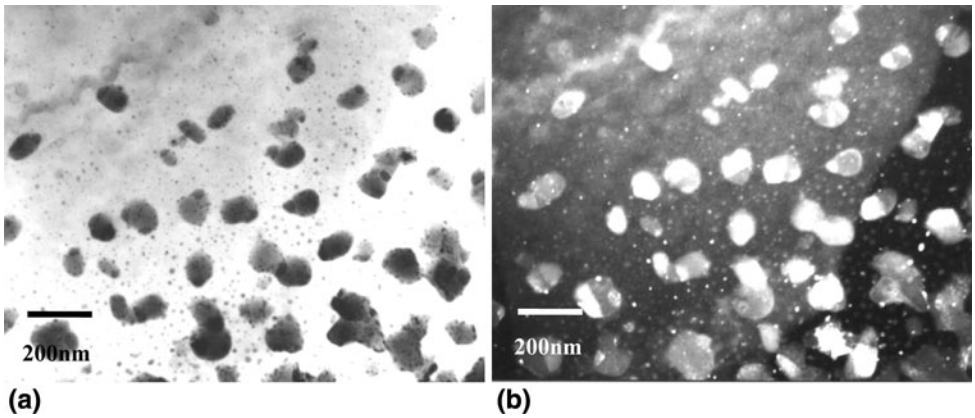

Fig. 3 TEM images showing dispersed nanocrystalline powder of alloy 1 (0.2 at.% Sn) on carbon-coated copper grid (a) bright field and (b) dark field images of same area. The presence of crystallites within particles is visible through diffraction contrast more prominent in dark field

The powder-grain size is determined by using XRD and TEM analysis. The grain size investigated by XRD "Integral Breadth method" reveals that there is a decreasing trend in grain size with increasing Sn contents as shown in Fig. 2.

Figure 3 shows TEM micrographs of alloy 1 showing a dispersion of coarse and fine nanocrystalline particles. Coarse particles exhibit diffraction contrast within their body mass, which is an indicative of multiple crystalline orientations in a single particle, having an average crystallite size of 26 nm. Similar observations are previously reported by other researchers as well (Ref 13, 18, 19). These results are within the size range required for exchange coupling (Ref 20).

The hysteresis loops of green compact samples with respect to Sn contents are shown in Fig. 4. It can be seen that the magnetization increases with increasing Sn contents, i.e., with decreasing crystallite size. However, the coercivity increases significantly when Sn contents was reduced from 1.1 (at.%) to 0.2 (at.%), the maximum coercivity of 787.8 kA/m (9.9 kOe) was achieved with Sn fraction of 0.2 (at.%). The magnetic properties seem to be influenced by the addition of Sn causing grain refinement and modification in crystallization behavior of the compounds as reported earlier (Ref 10-14, 21, 22).

It is also noted that there is a steady decrease in both M_r and M_{max} with reducing Sn concentration, i.e., with increasing crystallite size. The narrow difference between the values of M_r and M_{max} is the indicative of high M_r/M_{max} ratio, as it is shown in Fig. 5 and 6 which appears to be less sensitive to the Sn variations and subsequent grain refinement. The higher value of ratio M_r/M_{max} = 0.87-0.92 and grain size in the range of 18-35 nm, suggests the presence of intergranular exchange coupling phenomena (Ref 20, 23).

It should also be mentioned that all the hysteresis loops show a smooth demagnetization curves (Fig. 4), which also suggest exchange coupled uniform fine grains in the powders and contributing to remanence enhancement (Ref 24). The intergranular exchange coupling enhances with finer crystallite size and hence coercivity reduces with decreasing crystallite size or increasing Sn concentration as shown in Fig. 6 (Ref 21-23).

The coercivity decreases from 9.9 kO_e at faster rate with increasing Sn quantity to 350.2 kA/m (4.4 kO_e) (55% decrease) and then it decreases at slower rate to a value of 294.5 kA/m (3.7 kO_e) at 2.0 (at.%) Sn, (16% decrease) as shown in Fig. 6. Decreasing trend of coercivity and higher values of M_{max} with increasing Sn concentration can also be attributed toward more formation of 2:17 phase with *c*-axis orientation. This phase has low coercivity and higher saturation and higher quantities of it result in low coercive values (Ref 21, 23).

A coercivity of H_{ci} = 787.8 kA/m (9.9 kOe) and remanence ratio of M_r/M_{max} = 0.92 in alloy 1 reflect the presence of exchange coupling mechanism. The corresponding values of M_r and M_{max}, in comparison to alloys 2 and 3 are lower as shown in Fig. 5. It may be due to the increase in grain size as the amount of Sn is reduced as shown in Fig. 3. The higher remanence ratio in alloy 1 is probably due to the fact that the grain size still lies in the range to obtain higher M_r/M_{max} values, as reported in (Ref 22). The other possible reason for low remanence can be attributed to the further nucleation of 2:7 phase and declining amount of 2:17 phase with decreasing concentrations of Sn (Ref 25).

To evaluate the alignment effect on elevated M_r/M_{max} values, the samples of alloy 1 compacted in random orientation were tested for magnetic properties at the same parameters at which aligned compacts were characterized. The M_r/M_{max} values of aligned and randomly oriented samples were 0.92 and 0.91, respectively. These ratios indicate that the exchange coupling phenomena is present in both types of magnets. However, the maximum magnetization and remanence values are higher whereas coercivity is lower in aligned magnets as shown in Fig. 7. The increase in remanence and decrease in coercivity may be attributed to the effect of alignment (Ref 26).

It is observed that the Sn additions resulted in an in situ synthesis of nanocomposite magnets instead by mixing powders of hard and soft phases of the alloy (Ref 21) and increase in Sn concentration has resulted in refinement of in crystallite size in spite of similar milling conditions.

It is also reported that the switching field distribution (SFD) trend is also the indicative of exchange-coupled interactions (Ref 27-29). The second quadrant of hysteresis loop represents the magnetization reversal behavior of the material and the SFD is determined by taking first derivative of this curve. If SFD exhibits a single sharp peak (Gaussian distribution), then it is the indicative of uniformity of microstructure, i.e., only the magnetically hard phase or ideally exchanged coupled hard and soft phases in a nanocomposite magnet (Ref 27, 28). The behavior of SFD gives a clear diagnostic of variations in the microstructure, i.e., coexistence of soft and hard phases as well as nature and level of the exchange coupling.

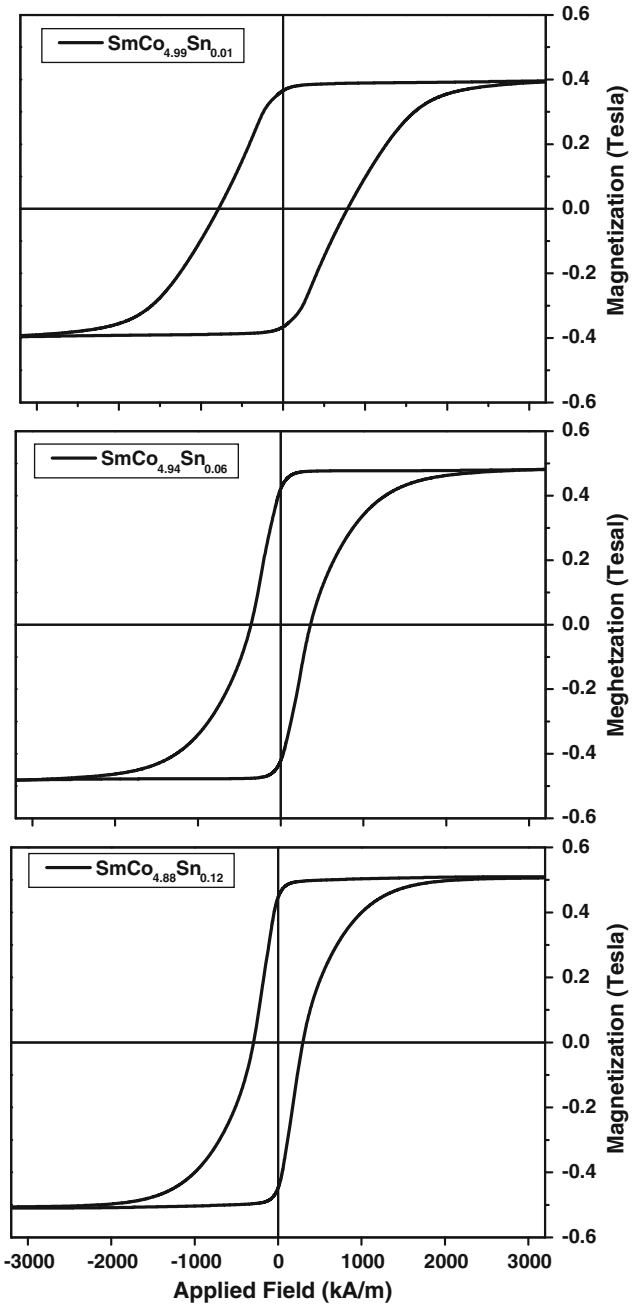

Fig. 4 Hysteresis loops of as-milled green compact samples showing the effect of Sn contents on the coercivity and magnetization in alloys 1-3

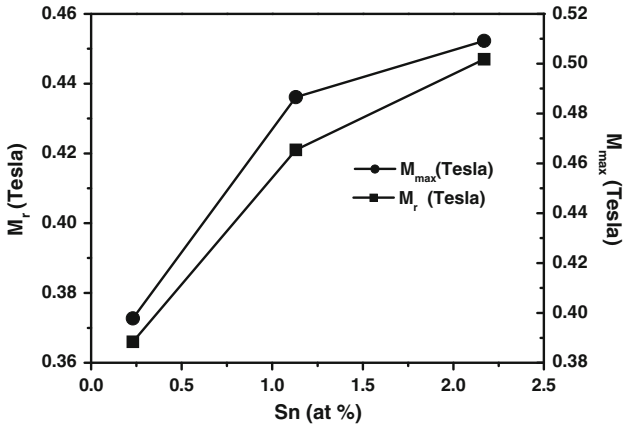

Fig. 5 Dependence of M_r and M_{max} on Sn contents in alloys 1-3

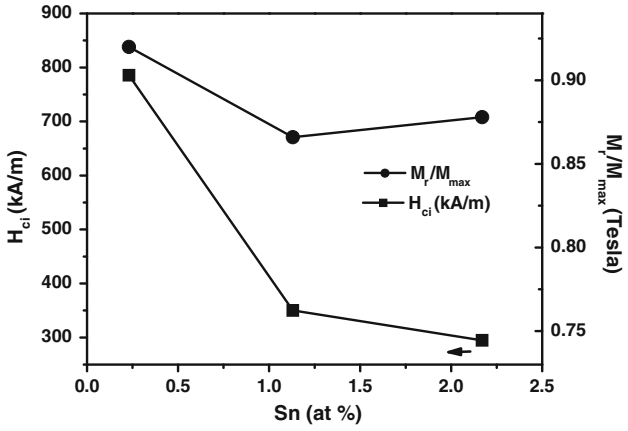

Fig. 6 Effect of Sn concentration on coercivity and M_r/M_{max} ratio in alloys 1-3

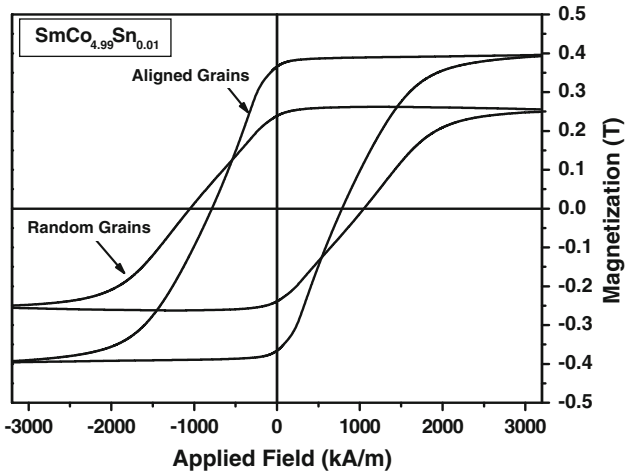

Fig. 7 Hysteresis loops of as-milled green compact samples showing the effect of the magnetic field aligning in alloy 1

Figure 8 shows SFD which reveals that the Sn addition has resulted in the exchange coupling phenomena and also indicates the magnetization reversals of hard and soft phases. H_{exch} is the point after that decoupling starts between hard and soft phases and corresponding demagnetizing field is called exchange coupling field (H_{exch}). Similarly, H_{irr} is irreversible demagnetizing field; beyond this point demagnetization is irreversible. The H_{exch} has shown insensitivity to variation in Sn concentration. H_{irr} is shifting to higher fields with decreasing Sn contents and H_{irr} is less than intrinsic coercivity (H_{ci}) for all the compositions. In exchange coupled two phase magnets the coercivity is lower and an optimization is necessary between the strength of exchange coupling and coercivity. The reduction in exchange coupling to a certain degree is required to optimize coercivity according to the application (Ref 30). It is revealed that the difference between the intrinsic coercivity (H_{ci}) and irreversible demagnetization (H_{irr}) is

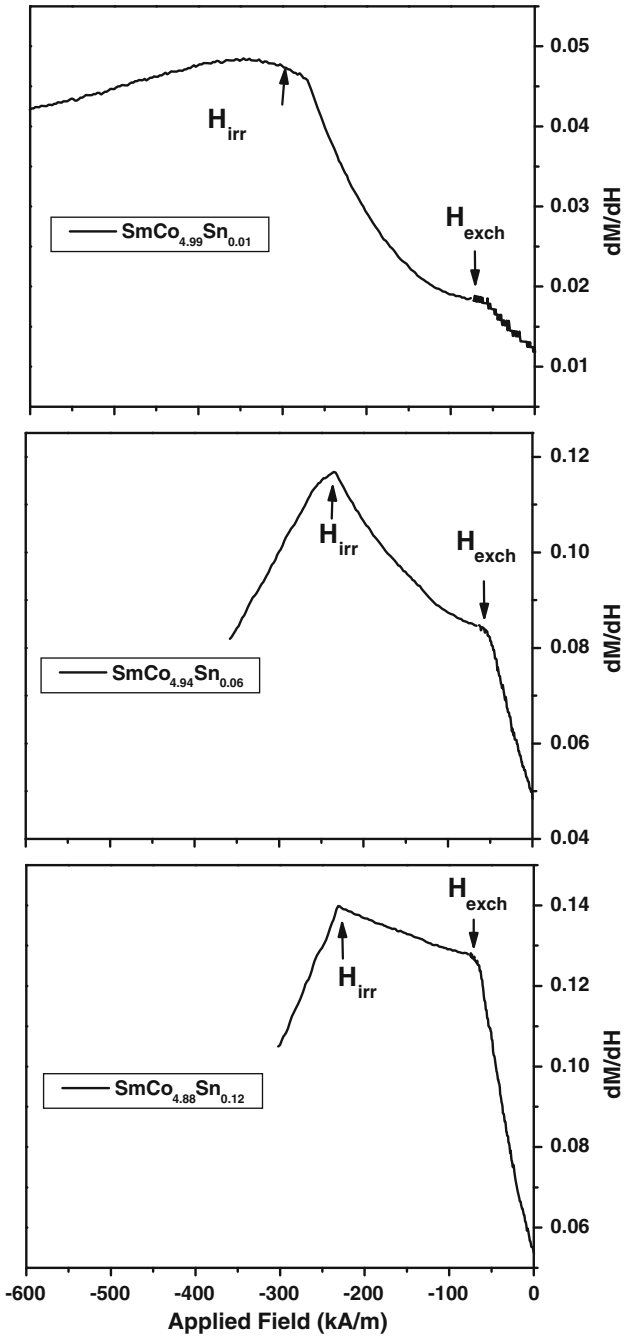

Fig. 8 Dependence of switching field distribution (SFD) (*dM*/*dH* of second quadrant demagnetization curves) on Sn contents for green compacts of alloys 1-3

increasing exponentially with decreasing Sn contents. The coercivity has shown the similar trend also. This may be attributed to the decreasing quantity of the soft phase as well as increase in grain size; similar behaviors have also been reported for two phase NdFeB/αFe melt spun ribbons by Chiriac et al. (Ref 31). The performance of exchange coupling depends on the stability of soft phase against the magnetization reversal (Ref 32). The region between H_{exch} and H_{irr} (Fig. 8) is an indicator of stiffness of soft phase to demagnetization. It appears to be less sensitive to the Sn concentration for alloys 2 and 3 but a comparative 30% increase for the alloy 1 was observed. It is the indicative of the reduction in the soft phase and consequently increases stiffness of the phase against the magnetization reversal. Alloy 1 has shown broader hump at the point of H_{irr} (Fig. 8) indicating retarded rate of demagnetization prior to the demagnetization avalanche, i.e., sluggish decoupling between hard and soft phases. It is pertinent to mention here that the intensities of the peaks for H_{irr} are higher than of H_{exch} peaks, which is the indication of presence of strong exchange coupling. In contrast, the reduction in coercivity with increasing Sn concentration can be attributed to increased soft phase, resulting in a reduction in resistance to demagnetization. The decrease in intensities of the both the H_{exch} and H_{irr} with reduction in Sn contents can also be attributed to the reduction in magnetization due to decreasing amount of soft phase. Similarly, the SFD peaks are getting sharper and higher with increasing Sn contents. This reflects more uniform distribution of the phases and finer grain size in samples (Ref 33).

4. Conclusions

The conclusions are summarized below:

- Increase in Sn concentration has resulted in refinement in the grain size to less than 20 nm under same milling conditions.
- Sn concentration is found to be influencing the crystallization of 2:17 and 2:7 phases in 1:5 matrix and helps in promoting the nucleation of 2:17 phase following the orientation of matrix phase.
- The narrow range of ratio M_r/M_{max} = 0.87-0.92 indicates its less sensitivity to the Sn variation. Decreasing trend in coercivity and SFD shows that increasing Sn is resulting in the enhanced intergranular exchange coupling phenomena.
- The aligned and randomly oriented compacts exhibited exchange coupling phenomena.
- The maximum coercivity of 787.8 kA/m (9.9 kOe) and high remanence ratio of 0.92 and SFD is reflecting exchange interactions between the nanocrystallites for 0.2 at.% Sn.
- SFD reveals the insensitivity of exchange coupling field (H_{exch}) to Sn contents. The increasing trend in irreversible demagnetization (H_{irr}) as well as increasing coercivity with decreasing Sn shows the ability to sustain higher demagnetizing field with optimum exchange coupling.
- In situ intergranular exchanged coupled nanocomposite magnets of high coercive 1:5 phase and higher magnetization 2:17 phases can be synthesized.

Acknowledgments

The authors are thankful to Prof. Dr. M. F. de Campos of EEIMVR-Universidade Fluminense, Avdos Trabalhadores, Brazil and Prof. Dr. R. William McCallum of Iowa State University Ames, USA for their helpful comments.

References

1. D.C. Jiles, Recent Advances and Future Directions in Magnetic Materials, *Acta Mater.*, 2003, **51**, p 5907–5939 (in English)
2. A. Menth, H. Negal, and R.S. Perkins, New High Performance Permanent Magnets Based on Rare Earth Transition Metal Compounds, *Ann. Rev. Mater. Sci.*, 1978, **8**, p 21–47 (in English)

3. O. Gutfleisch, Controling the Properties of High Energy Density Permanent Magnetic Materials by Different Processing Routes, *J. Phys. D Appl. Phys.*, 2003, **33**, p R157–R172 (in English)
4. K.J. Strant, Cobalt-Rare Earth Alloys as Promising New Permanent Magnet Materials, *Cobalt*, 1967, **9**(36), p 133–143 (in English)
5. V.P. Menushenkov, Phase Transformation and Coercivity in Rare-Earth Permanent Magnets, *J. Magn. Magn. Mater.*, 2005, **290–291**, p 174–1277 (in English)
6. M.F. de Campos, F.J.G. Landgraf, N.H. Saito, S.A. Romero, A.C. Neiva, F.P. Missell, E. de Morais, S. Gama, E.V. Obrucneva, and B.V. Jalnin, Chemical Composition and Coercivity of $Smco_5$ Magnets, *J. Appl. Phys.*, 1998, **84**(1), p 368–373 (in English)
7. E.A. Nesbit, New Permanent Magnetic Materials containing Rare Earth Metals, *J. Appl. Phys.*, 1969, **40**, p 1259–1265 (in English)
8. Y. Zhang, A. Gabay, Y. Wang, and G.C. Hadjipanayis, Microstructure, Microchemistry, and Coercivity in Sm-Co-Cu and Pr-Co-Cu Alloys, *J. Magn. Magn. Mater.*, 2004, **272–276**, p 1899–1900 (in English)
9. A.M. Gaby, P. Larson, I.I. Mazin, and G.C. Hadjipanayis, Magnetic States and Structural Transformation in $Sm(Co, Cu)_5$ and $Sm(Co, Fe, Cu)_5$ Permanent Magnets, *J. Phys. D Appl. Phys.*, 2005, **38**, p 1337–1341 (in English)
10. S. Washko, J. Gerboc, and J. Orehotsky, Magnetic and Crystallographic Properties of SmCo Based Ternary Alloys, *IEEE Trans. Magn. Mag.*, 1976, **12**(6), p 974–976 (in English)
11. A.A. Kundig, R. Goplan, T. Ohkubo, and K. Hono, Coercivity Enhancement in Melt-Spun $SmCo_5$ by Sn Addition, *Scr. Mater.*, 2006, **54**, p 2047–2051 (in English)
12. M.L. Kahn, J.-L. Bobet, F. Weill, and B. Chevalier, Modification of the Magnetic Properties of $SmCo_5$ Particles Depending on the Grinding Atmosphere, *J. Alloys Compd.*, 2002, **334**, p 285–292
13. N. Tang, Z. Chen, Y. Zhang, G.C. Hadjipanayis, and F. Yang, Nanograined YCo_5-Based Powders with high Coercivity, *J. Magn. Magn. Mater.*, 2000, **219**, p 173–177 (in English)
14. G.C. Hadjipanayis, Nanophase Hard Magnets, *J. Magn. Magn. Mater.*, 1999, **200**, p 373–391 (in English)
15. K.M. Choadary, A.K. Glri, K. Pellerin, S.A. Majetich, and J.H.J. Scott, Annealing effect on the Coercivity of $SmCo_5$ Nanoparticles, *J. Appl. Phys.*, 1999, **85**(8), p 4331–4333 (in English)
16. H.P. Klug and L.E. Alexander, *Method of Integral Breadths, X-ray Diffraction Procedures for Polycrystalline and Amorphous Materials*, 2nd ed., Wiley, New York, 1974, p 661–665 (in English)
17. Z.D. Zhang, W. Liu, J.P. Liu, and D.J. Sellmyer, Metastable Phases in Rare-Earth Permanent-Magnet Materials, *J. Phys. D Appl. Phys.*, 2000, **33**, p R217–R246 (in English)
18. C. Orquiz-Mela, J.A. Matutes-Aquino, Nanocrystalline $Pr_{0.5}Sm_{0.5}Co_5$ Alloy obtained by Mechanical Milling, *J. Magn. Magn. Mater.*, 2008, doi: 10.1016/j.jmmm.2008.02.123 (in English)
19. J.T. Elizalde Galindo, H.A. Davies, and J.A. Matutes-Aquino, Structural and Magnetic Properties of Mechanically Milled $Y_{1-x}Pr_xCo_5$ compounds [x = 0, 0.1, 0.3, 0.5], *Mater. Charact.*, 2007, **58**, p 805–808 (in English)
20. H.A. Davies, Nanocrystalline Exchange-Enhanced Hard Magnetic Alloys, *J. Magn. Magn. Mater.*, 1996, **157/158**, p 11–14 (in English)
21. Z. Chen, Y. Zhang, and G.C. Hadjipanayis, Nanocomposite $PrCo_5$/Pr_2Co_{17} Magnets With Enhanced Maximum Energy Product, *J. Magn. Magn. Mater.*, 2000, **219**, p 178–182 (in English)
22. W. Rave and K. Ramstock, Micromagnetic Calculation of the Grain size dependence of Remanence and Coercivity in Nanocrystalline Permanent Magnets, *J. Magn. Magn. Mater.*, 1997, **171**, p 69–82 (in English)
23. R. Skomski, J.M.D. Coey, *Permanent Magnetism*, Institute of Physics Publishing, Bristol, Philadelphia, 1999, p 186–191, 298–301
24. K.H.J. Buschow, *Handbook of Magnetic Materials*, Vol 10, Elsevier, North-Holland, New York, 1997, p 503–504 (in English)
25. M.F. de Campos, F.J.G. landgral, R. Machado, D. Rodringues, S.A. Romero, A.C. Neiva, and F.P. Missell, A Model relating Remanence and Microstructure of $SmCo_5$ Magnets, *J. Alloys Compd.*, 1998, **267**, p 257–264 (in English)
26. R.W. Gao, D.H. Zhang, W. Li, X.M. Li, and J.C. Zhang, Hard Magnetic property and δM(H) plot for Sintered NdFeB Magnet, *J. Magn. Magn. Mater.*, 2000, **208**, p 239–243 (in English)
27. R.W. McCallum, Determination of the Saturation Magnetization, Anisotropy Field, Mean Field Interaction, and Switching Field Distribution for Nanocrystalline Hard Magnets, *J. Magn. Magn. Mater.*, 2005, **292**, p 135–142 (in English)
28. K. Kang, L.H. Lewis, J.S. Jiang, and S.D. Bader, Recoil Hysteresis of Sm-Co/Fe Exchange-Spring Bilayers, *J. Appl. Phys.*, 2005, **98**, p 1139061–1139067 (in English)
29. Y. Kato and M. Tsutsumi, An Analysis of Magnetization Reversal Process, *IEEE. Trans. Magn.*, 1992, **28**(5), p 2686–2688
30. T. Schrefl, J. Fidler, and D. Suss, *Micromagnetic Modeling of Nanocomposite Magnets*, Institute of Applied and Technical Physics, Vienna University of Technology, Wiedner Hauptstraβe 8-1040 Vienna, Austria (in English)
31. H. Chiriac, M. Marinescu, P. Tiberto, and F. Vinai, Reversible Magnetization Behavior and Exchange Coupling in Two-Phase NdFeB Melt Spun Ribbons, *Mater. Sci. Eng. A*, 2001, **304–306**, p 957–960 (in English)
32. J.S. Jiang, H.G. Kaper, and G.K. Leaf, Hysteresis in Layered Spring Magnets, *Discret. Contin. Dyn. Syst. Ser. B*, 2001, **1**(2), p 219–232 (in English)
33. Y. Gao, J. Zhu, Y. Weng, E.B. Park, and C.J. Yang, The Enhanced Exchange Coupled Interaction in Nanocrystalline $Nd_2Fe_{14}B/Fe_3B$ + αFe Alloys With Improved Microstructure, *J. Magn. Magn. Mater.*, 1999, **191**, p 146–152 (in English)